

SUSY Discovery Potential and Benchmarks for Early Runs at $\sqrt{s} = 7$ TeV at the LHC

Baris Altunkaynak,^{*} Michael Holmes,[†] Pran Nath,[‡] Brent D. Nelson,[§] and Gregory Peim[¶]

Department of Physics, Northeastern University, Boston, Massachusetts 02115, USA

We carry out an analysis of the potential of the Large Hadron Collider (LHC) to discover supersymmetry in runs at $\sqrt{s} = 7$ TeV with an accumulated luminosity of $(0.1-2) \text{ fb}^{-1}$ of data. The analysis is done with both minimal supergravity and supergravity models with nonuniversal soft breaking. Benchmarks for early discovery with $(0.1-2) \text{ fb}^{-1}$ of data are given. We provide an update of b-tagging efficiencies in PGS 4 appropriate for LHC analyses. A large number of signature channels are analyzed and it is shown that each of the models exhibited are discoverable at the 5σ level or more above the standard model background in *several* signature channels which would provide cross checks for a discovery of supersymmetry. It is shown that some of the benchmarks are discoverable with 0.1 fb^{-1} of data again with detectable signals in several channels.

PACS numbers: 12.60.Jv, 14.80.Ly, 95.35.+d

I. INTRODUCTION

The Large Hadron Collider (LHC) is currently running and collecting data at $\sqrt{s} = 7$ TeV. It is expected that it would continue until it has collected at least 1 fb^{-1} of integrated luminosity. It is then interesting to investigate the discovery potential of LHC for supersymmetry (SUSY) in these early runs.¹ Some work in this direction has already been done [2–7]. We carry out the analysis of the SUSY discovery potential of the LHC using the next-to-lightest supersymmetric partner (NLSP) as a discriminant of models. Several possibilities arise, the most dominant of which involve a χ^\pm , $\tilde{\tau}$, \tilde{t} , CP odd Higgs A or \tilde{g} as the NLSP. As is well known, the parameter space of minimal supersymmetric standard model (MSSM) is very large, consisting of more than a hundred parameters, and thus an analysis within this full space of MSSM is intractable. This space is significantly reduced in well motivated models such as the minimal supergravity model (mSUGRA) where one assumes R parity invariance and defines the symmetry breaking parameters at the grand unification (GUT) scale. These are evolved to low scales by renormalization group evolution where the entire sparticle spectrum is determined in terms of the GUT scale parameters. Specifically in mSUGRA under the constraint of R parity one has four parameters and one sign [see Eq.(3)] and in nonuniversal supergravity models with nonuniversalities in the gaugino sector the space is extended to six parameters and a sign. The allowed parameter space is subjected to further theoretical and experimental constraints, i.e., constraints of radiative electroweak symmetry breaking (REWSB) with color and charge conservation, satisfaction of flavor changing neutral current (FCNC) constraints, and experimental lower limit constraints on the Higgs masses and on the masses of the sparticles. Further, in supergravity unified models under the constraints of R parity invariance the lowest R parity odd particle (LSP) turns out to be the neutralino over a large part of the parameter space and thus a possible candidate for dark matter. Imposition of the WMAP constraint and constraints from direct detection of dark matter further reduce the allowed parameter space in these supergravity models.

However, even after the imposition of all the constraints the allowed parameter space is still large and additional criteria must be used in model selection for a study of their signatures. This study is focussed on SUSY discovery in the early runs at the LHC, i.e., at $\sqrt{s} = 2$ TeV with $(1-2) \text{ fb}^{-1}$ of integrated luminosity. Obviously then it makes sense to choose those SUSY models which can be explored within the parameters of the data that will be collected in these early runs. However, within this general rubric one ought to make the search as large as possible. For example, there is no theoretical necessity to limit our analysis exclusively to just one region of REWSB such as just to the stau coannihilation branch. Thus in our analysis, under the constraint that the model points we explore be observable in the early runs, we search for a diverse set of models where the NLSP could be one of the allowed set by REWSB. For

* altunkaynak.i@husky.neu.edu

† holmes.mi@neu.edu

‡ nath@neu.edu

§ b.nelson@neu.edu

¶ peim.g@husky.neu.edu

¹ For a review of the discovery potential at $\sqrt{s} = 14$ TeV and $\sqrt{s} = 10$ TeV see [1] and the references therein.

A display of the processes analyzed and their standard model backgrounds at $\sqrt{s} = 7$ TeV

SM process	Cross section (fb)	Number of events	Luminosity (fb^{-1})
QCD 2, 3, 4 jets (Cuts1)	2.0×10^{10}	74M	3.7×10^{-3}
QCD 2, 3, 4 jets (Cuts2)	7.0×10^8	98M	0.14
QCD 2, 3, 4 jets (Cuts3)	4.6×10^7	40M	0.88
QCD 2, 3, 4 jets (Cuts4)	3.9×10^5	1.7M	4.4
$t\bar{t} + 0, 1, 2$ jets	1.6×10^5	4.8M	30
$b\bar{b} + 0, 1, 2$ jets	9.5×10^7	95M	1.0
$Z/\gamma (\rightarrow \ell\bar{\ell}, \nu\bar{\nu}) + 0, 1, 2, 3$ jets	6.2×10^6	6.2M	1.0
$W^\pm (\rightarrow \ell\nu) + 0, 1, 2, 3$ jets	1.9×10^7	21M	1.1
$Z/\gamma (\rightarrow \ell\bar{\ell}, \nu\bar{\nu}) + t\bar{t} + 0, 1, 2$ jets	56	1.0M	1.7×10^4
$Z/\gamma (\rightarrow \ell\bar{\ell}, \nu\bar{\nu}) + b\bar{b} + 0, 1, 2$ jets	2.8×10^3	0.1M	36
$W^\pm (\rightarrow \ell\nu) + b\bar{b} + 0, 1, 2$ jets	3.2×10^3	0.6M	1.8×10^2
$W^\pm (\rightarrow \ell\nu) + t\bar{t} + 0, 1, 2$ jets	70	4.6M	6.5×10^4
$W^\pm (\rightarrow \ell\nu) + t\bar{b} (\bar{t}b) + 0, 1, 2$ jets	2.4×10^2	2.1M	8.7×10^3
$t\bar{t}\bar{t}$	0.5	0.09M	1.8×10^5
$t\bar{t}b\bar{b}$	1.2×10^2	0.32M	2.7×10^3
$b\bar{b}b\bar{b}$	2.2×10^4	0.22M	1.0
$W^\pm (\rightarrow \ell\nu) + W^\pm (\rightarrow \ell\nu)$	2.0×10^3	0.05M	25
$W^\pm (\rightarrow \ell\nu) + Z (\rightarrow \text{all})$	1.1×10^3	1.3M	1.1×10^3
$Z (\rightarrow \text{all}) + Z (\rightarrow \text{all})$	7.3×10^2	2.6M	3.6×10^3
$\gamma + 1, 2, 3$ jets	1.5×10^7	16M	1.1

TABLE I: An exhibition of the standard model backgrounds computed in this work at $\sqrt{s} = 7$ TeV. All processes were generated using MadGraph 4.4 [12]. Our notation here is that $\ell = e, \mu, \tau$, and $\text{all} = \ell, \nu, \text{jets}$. Cuts1-Cuts4 indicated in the table are defined in Eq. (1). In the background analysis we eliminate double counting between the process $W^\pm + t\bar{b} (\bar{t}b)$ and $t\bar{t}$ by subtracting out double resonant diagrams of $t\bar{t}$ when calculating $W^\pm + t\bar{b} (\bar{t}b)$.³

the analysis we present here we find this set to be a chargino (χ^\pm), a stau ($\tilde{\tau}$), a gluino (\tilde{g}), CP odd Higgs (A^0), and a stop (\tilde{t}). Thus in the analysis of this paper we give several benchmarks with this diverse set of NSLPs. It should be kept in mind that there is still a significant amount of subjectivity in the choice of the benchmarks. To mitigate the subjective element in the choice of the benchmarks we further choose the input parameters to be as diverse as possible. The investigation is done both for mSUGRA as well as for models with nonuniversalities. The outline of the rest of the paper is as follows: In Sec. (II) we discuss the analysis of standard model backgrounds at $\sqrt{s} = 7$ TeV. In Sec. (III) we give an analysis of the cross sections for the production of various sparticle processes. These include the production of gluinos and squarks, production of a combination of gluinos and charginos or neutralinos, and production of charginos and neutralinos. In Sec. (IV) we give an analysis of possible signatures, discuss the SUSY discovery potential and give reach plots of the LHC early runs. In Sec. (V) we give several benchmarks consistent with all current constraints which are possible candidates for early discovery. Conclusions are given in Sec. (VI) and larger tables have been relocated to Sec. (VII).

II. ANALYSIS OF STANDARD MODEL BACKGROUNDS AT $\sqrt{s} = 7$ TEV

A central element in the discovery of new physics is the determination of the standard model (SM) backgrounds for the processes where one expects to see new physics. One such analysis at $\sqrt{s} = 7$ TeV has already appeared in the literature [4].² Here we give an independent analysis of the relevant backgrounds. In our analysis, we use MadGraph 4.4 [12] for parton level processes, Pythia 6.4 [13] for hadronization, and PGS 4 for detector simulation [14]. We used MLM matching with a k_T jet clustering scheme to prevent double counting of final states. Furthermore, the b -tagging efficiency of PGS 4 was updated to better represent the analysis at the LHC. A discussion of this improvement is given below. The result of our analysis is presented in Table (I) with parton level cuts as specified in Eq. (1) and in the caption of Table (I). Our analysis compares well with the analysis of [4]. The differences between the two analyses are in part due to the differences between matrix-element Monte Carlo generators which are known to

² For some previous works on early discovery though at higher energies see [2, 8–11]

A comparison of b -tagging efficiency in PGS 4 vs ATLAS detectors

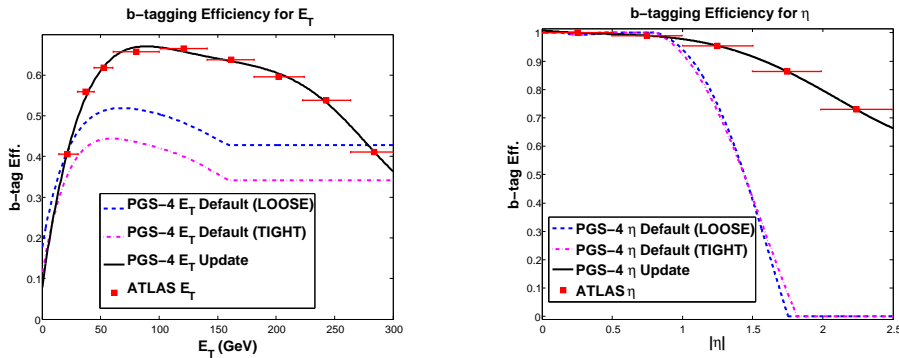


FIG. 1: Left panel: A comparison of the b -tagging efficiency of ATLAS and the loose and tight efficiencies of PGS 4 as a function of E_T . Right panel: A comparison of the b -tagging efficiency of ATLAS and the loose and tight efficiencies of PGS 4 as a function of η . Ours fits to the efficiency of ATLAS as a function of E_T , and η as parametrized by Eq. (2) are also exhibited.

exist [15]. For example, we have exclusively used MadGraph with a k_T -based jet clustering algorithm in our analysis, while AlpGen [16] uses a cone-based jet clustering algorithm and was the dominant tool used in [4]. In the analysis here we have used CTEQ6L1 [17] parton distribution functions for generating the SM background, and a basic cut was applied such that all final state partons (except the top quarks) are required to have $p_T > 40$ GeV.

$$\begin{aligned} \text{Cuts1} &= 40 \text{ GeV} < E_T(j_1) < 100 \text{ GeV}, & \text{Cuts2} &= 100 \text{ GeV} < E_T(j_1) < 200 \text{ GeV}, & \text{Parton level} \\ \text{Cuts3} &= 200 \text{ GeV} < E_T(j_1) < 500 \text{ GeV}, & \text{Cuts4} &= 500 \text{ GeV} < E_T(j_1) < 3000 \text{ GeV} & \text{cuts.} \end{aligned} \quad (1)$$

An important object in many possible SUSY discovery channels is a b -tagged jet. In PGS 4 b tagging is done based off of the Tevatron b -tagging efficiency. However, it is pertinent to ask if this is a valid approximation of what is to be expected at the LHC. Using the Technical Design Reports (TDR) of CMS [18] and of ATLAS [19] one can extract the expected b -tagging efficiency as a function of jet pseudorapidity, η , and transverse energy E_T for jets originating from heavy-flavor partons. In Fig. (1) we give a comparison of the functions given in the ATLAS TDR [18, 19] with the one given in PGS 4. We have omitted the CMS data, since in the TDR b tagging is binned into two sets of η so one could not extract a continuous function from it. The left panel of Fig. (1) gives the b -tagging efficiencies as a function of E_T for ATLAS and the so called “tight” and “loose” efficiencies as defined in PGS 4. One finds a significant difference between these and those expected in the ATLAS and CMS detectors. A similar analysis but as a function of η is given in the right panel of Fig. (1) where the difference between the efficiencies given by PGS 4 and by (normalized) ATLAS is even more glaring. For this analysis, we do not extend the definition of b -tagging beyond η of 2.0. Previously, b -tagging efficiencies were assumed to approach a constant value for $E_T \geq 160$ GeV. We have extended this such that the tagging efficiency reaches a constant for $E_T \geq 300$ GeV. Thus we have updated b -tagging functions as given in Eq. (2) where we have kept the same degree polynomial as the preexisting b -tagging functions in PGS 4. Furthermore, the total b -tagging efficiency is the product of the E_T and η functions listed in Eq. (2). Here we make no modification to the default PGS 4 rate for mistagging b jets. Our revised b -tagging functions have the form

$$\begin{aligned} b_{E_T} &= 0.0781391 + 0.0202661E_T - 0.000259664E_T^2 + 1.5509 \times 10^{-6}E_T^3 - 4.46698 \times 10^{-9}E_T^4 + 4.7995 \times 10^{-12}E_T^5 \\ b_\eta &= 1.00885 - 0.0497485\eta + 0.693036\eta^2 - 0.0361142\eta^3 - 0.0222204\eta^4 + 0.00797621\eta^5. \end{aligned} \quad (2)$$

III. SPARTICLE PRODUCTION CROSS SECTIONS AT $\sqrt{s} = 7$ TEV

The soft breaking sector of the MSSM is rather large consisting of over a hundred arbitrary parameters. Here we use the framework of high scale supergravity to reduce this arbitrariness. Thus, for the supergravity grand unified

³ When studying $W + t\bar{b}$ ($t\bar{b}$) processes there is a potential to double count such final states if one also considers t, \bar{t} production processes. To prevent this double counting we have eliminated all diagrams involving a top quark from the set of diagrams that lead to $W + t\bar{b}$ final states, with an analogous requirement for $W + t\bar{b}$ production.

Sparticle Production Cross Sections of mSUGRA at $\sqrt{s} = 7$ TeV

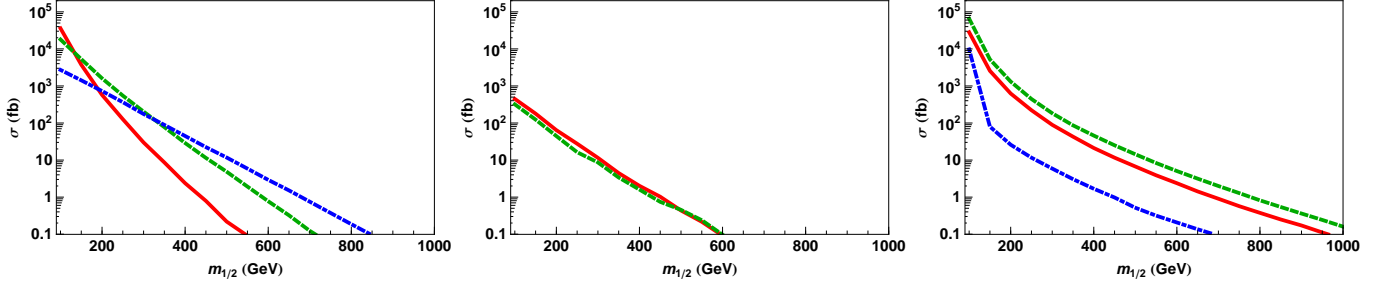


FIG. 2: An exhibition of the sparticle production cross sections at the LHC at $\sqrt{s} = 7$ TeV for mSUGRA as a function of the universal gaugino mass $m_{1/2}$ at the GUT scale when $m_0 = 500$ GeV, $A_0 = 0$, $\tan\beta = 20$ and $\text{sign}(\mu) = +1$. Left panel: production cross sections of $\tilde{g}\tilde{g}$, $\tilde{g}\tilde{q}$, $\tilde{q}\tilde{q}$ (solid red, dashed green, dashed blue lines). Middle panel: production cross sections for $\tilde{g}\chi^\pm$, $\tilde{g}\chi^0$ (solid red, dashed green lines). Right panel: production cross sections for $\chi^\pm\chi^\pm$, $\chi^\pm\chi^0$, $\chi^0\chi^0$ (solid red, dashed green, dashed blue lines).

model with universal soft breaking, i.e., mSUGRA [20], one has just four parameters and the sign of the Higgs mixing parameter μ ; i.e., one has

$$m_0, m_{\frac{1}{2}}, A_0, \tan\beta, \text{sign}(\mu), \quad (3)$$

where m_0 is the universal scalar mass, $m_{\frac{1}{2}}$ is the universal gaugino mass, A_0 is the coefficient of the trilinear coupling, and $\tan\beta$ is the ratio of two Higgs vacuum expectation values in the MSSM. Since the nature of physics at the Planck scale is still largely unknown, one may extend the minimal supergravity model to include nonuniversalities in the gaugino and Higgs sectors as well as in the flavor sector consistent with the FCNC constraints. One of the most widely used extensions of mSUGRA consists of the inclusion of nonuniversalities in the gaugino sector [21–27]. Thus one may include these nonuniversalities by parametrizing the gaugino masses at the grand unified scale, which we take to be 10^{16} GeV, via the relations $\tilde{m}_i = m_{1/2}(1 + \delta_i)$ ($i=1,2,3$) corresponding to the gauge groups $U(1)$, $SU(2)_L$, and $SU(3)_C$.

In this framework, the model points are generated by the imposition of REWSB, particle mass limits from LEP and the Tevatron, relic density constraints from WMAP [28], the $g_\mu - 2$ constraints, and FCNC constraints from $B_s \rightarrow \mu^+\mu^-$ and $b \rightarrow s + \gamma$. WMAP has measured $\Omega_{DM}h^2$ to a great accuracy with $\Omega_{DM}h^2 = 0.1109 \pm 0.0056$ [28]. However, to account for the errors in the theoretical computations and possible variations in the computation of the relic density using different codes we take a rather wide range in the relic density constraints, i.e., $0.06 < \Omega_{DM}h^2 < 0.16$, in our analysis. Regarding the $g_\mu - 2$ constraint [29] recent analysis of the hadronic corrections [30] indicate a significant deviation around 3.9σ between the SM prediction and experiment. Such a contribution can arise from supersymmetry [31] and the size of the correction indicates the supersymmetric particles (sparticles) to be low in mass.

For the FCNC process $B_s \rightarrow \mu^+\mu^-$ we take the constraint to be $\mathcal{BR}(B_s \rightarrow \mu^+\mu^-) < 5.8 \times 10^{-8}$ [32, 33] and for the process $b \rightarrow s\gamma$ we take the constraint to be $\mathcal{BR}(b \rightarrow s\gamma) = (352 \pm 34) \times 10^{-6}$ [34, 35]. We note in passing that currently there is a small discrepancy between the SM prediction and the experimental result for $b \rightarrow s\gamma$ which is a possible hint for the SUSY contribution [36] and hence another indication of possible low-lying sparticle masses. Thus this discrepancy along with the reported $g_\mu - 2$ result is encouraging for an early SUSY discovery [37]. In addition to the above, LEP and Tevatron mass constraints on the sparticle masses and on the Higgs masses are applied. These are $m_A > 85$ GeV, $m_{H^\pm} > 79.3$ GeV, $m_{\tilde{t}_1} > 101.5$ GeV, and $m_{\tilde{\tau}_1} > 98.8$ GeV where A is the CP odd Higgs and H^\pm is the charged Higgs. Further, we impose the lightest CP even Higgs mass constraint [38] $m_h > (93.5 + 15x + 54.3x^2 - 48.4x^3 - 25.7x^4 + 24.8x^5 - 0.5)$ GeV where $x = \sin^2(\beta - \alpha)$ and α is the Higgs mixing angle. The final term in the bound represents a theoretical error of 0.5 GeV in the calculation of M_h and M_A assumed by the authors of Ref. [38]. Additionally we use the constraints $m_{\chi_1^\pm} > 104.5$ GeV if $|m_{\chi_1^\pm} - m_{\chi_1^0}| > 3$ GeV for the chargino mass and $m_{\tilde{g}} > 309$ GeV for the gluino mass [33]. In the analysis we use a top (pole) mass of $m_t = 173.1$ GeV. Finally, we also apply the constraint that the model points are consistent with recent data from CDMS-II [39] and XENON-100 [40]. Using MicrOMEGAs 2.4 [41] the spin independent neutralino-proton cross section was calculated and compared to CDMS-II and XENON-100. Furthermore, we compare our results to the expected sensitivity for XENON-100 6000 kg \times day and XENON-1Ton for 1 ton \times year [42] as well as the expected sensitivity for SuperCDMS [43].

Contours of σ_{SUSY} in the $m_{\tilde{g}} - m_{\chi_{\pm}^1}$ mass plane at $\sqrt{s} = 7$ TeV

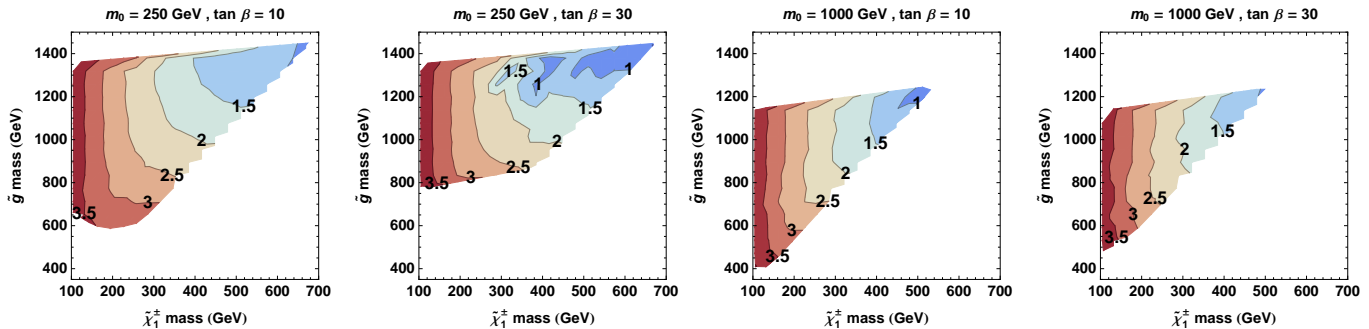


FIG. 3: Contour plots with constant values of $\log(\sigma_{SUSY}/\text{fb})$ for σ_{SUSY} in $m_{\tilde{g}} - m_{\chi_{\pm}^1}$ mass plane for the case with nonuniversalities in the gaugino sector. Gaugino masses m_1 , m_2 , and m_3 vary up to 1 TeV. First panel from left: $m_0 = 250$ GeV, $\tan \beta = 10$ while $A_0 = 0$, $\text{sign}(\mu)=+1$; second panel from left: $m_0 = 250$ GeV, $\tan \beta = 30$; third panel from left: $m_0 = 1000$ GeV, $\tan \beta = 10$; fourth panel from left: $m_0 = 1000$ GeV, $\tan \beta = 30$.

Next we present the cross sections for sparticle production processes in mSUGRA calculated from Pythia 6.4 at $\sqrt{s} = 7$ TeV. This is done by generating 5K events for multiple $m_{1/2}$ values where the other parameters are taken to be $m_0 = 500$ GeV, $A_0 = 0$, $\tan \beta = 20$, and $\mu > 0$. The results are exhibited in Fig. (2) where the left panel gives the cross sections for the production of $\tilde{g}\tilde{g}$ (solid red line), $\tilde{g}\tilde{q}$ (dashed green line), $\tilde{q}\tilde{q}$ (dashed blue line) as a function of $m_{1/2}$. The middle panel gives the cross sections for the production of $\tilde{g}\chi^{\pm}$ (solid red line), $\tilde{g}\chi^0$ (dashed green line), and the right panel gives the production cross section for $\chi^{\pm}\chi^{\pm}$ (solid red line), $\chi^{\pm}\chi^0$ (dashed green line), $\chi^0\chi^0$ (dashed blue line). The analysis of Fig. (2) shows these cross sections to be significant, indicating that at low mass scales as many as 10^4 or more SUSY events will be generated with 1 fb^{-1} of integrated luminosity at the LHC. A similar analysis for the case with nonuniversalities in the gaugino mass sector is given in Fig. (3), where we give contour plots in the $m_{\tilde{g}} - m_{\chi_{\pm}^1}$ mass plane with other parameters as stated in the caption of the figure. The plots give contours of constant $\log(\sigma_{SUSY}/\text{fb})$ in the range 1 – 3.5. The contours' plots indicate that a chargino mass up to about 500 GeV and a gluino mass up to roughly 1 TeV would give up to 10^3 or more events with 1 fb^{-1} of integrated luminosity. Of course, the discovery of sparticles requires an analysis including the backgrounds and selection of appropriate cuts to enhance the signal to the background ratio. This will be discussed in Secs. (IV) and (V).

IV. SIGNATURE ANALYSIS AND SUSY DISCOVERY REACH AT $\sqrt{s} = 7$ TEV AND 1 FB^{-1}

A number of works already exist which analyze the signatures for supersymmetry at $\sqrt{s} = 14$ TeV and $\sqrt{s} = 10$ TeV (for a small sample see [9–11, 44]). In our analysis we computed the sparticle branching ratios with SUSY-HIT [45] and they were subsequently read into Pythia. PGS 4 was used for the detector simulation with no trigger imposed (L0). Here we give the analysis for $\sqrt{s} = 7$ TeV for a large number of signatures for each candidate model considered. These are listed in Table (II) and consist of a combination of multijets, b-tagged jets, multileptons, jets and leptons, and photons with a variety of cuts geared to reduce the standard model background and enhance the SUSY signal with and without missing energy. We discuss first the model with universal soft breaking, i.e., the mSUGRA model. In Fig. (4) we give the reach of the early runs at the LHC for mSUGRA in the $m_{1/2} - m_0$ plane. One finds that the reach can extend up to about 400 GeV for $m_{1/2}$ at low values of m_0 and up to about 2 TeV for m_0 for low values of $m_{1/2}$ with 1 fb^{-1} of integrated luminosity, and up to about 450 GeV for 2 fb^{-1} of data, and for m_0 the reach can extend up to 1.9 (2) TeV for $1(2)\text{fb}^{-1}$ of integrated luminosity. For the nonuniversal case a plot in $m_{1/2} - m_0$ is not very illuminating because of the presence of nonuniversalities. Here we exhibit in Table (III) a set of benchmarks which have a chance of early discovery. A criterion used in the selection of these benchmarks is the size of the cross section for the production of SUSY events σ_{SUSY} which is shown in the last column of Table (III). Here one finds that σ_{SUSY} for some of the benchmarks is as large as 10-20 pb or more implying that as many as $(1 - 2) \times 10^4$ SUSY events will be produced at the LHC with 1 fb^{-1} of integrated luminosity. Thus with efficient cuts to reduce the SM background there appears a good chance for the discovery of such models. A detailed analysis of the signatures implementing the cuts of Table (II) bears this out. Thus as exhibited in Fig. (5) one finds that all of the benchmarks of Table (III) do indeed produce visible signals not just in one but in several channels. In fact for most the benchmark models of Table (III) one has as many as five channels and often more where the SUSY signal will become visible, thus

Reach Plot at $\sqrt{s} = 7$ TeV up to 2 fb^{-1} of Integrated Luminosity.

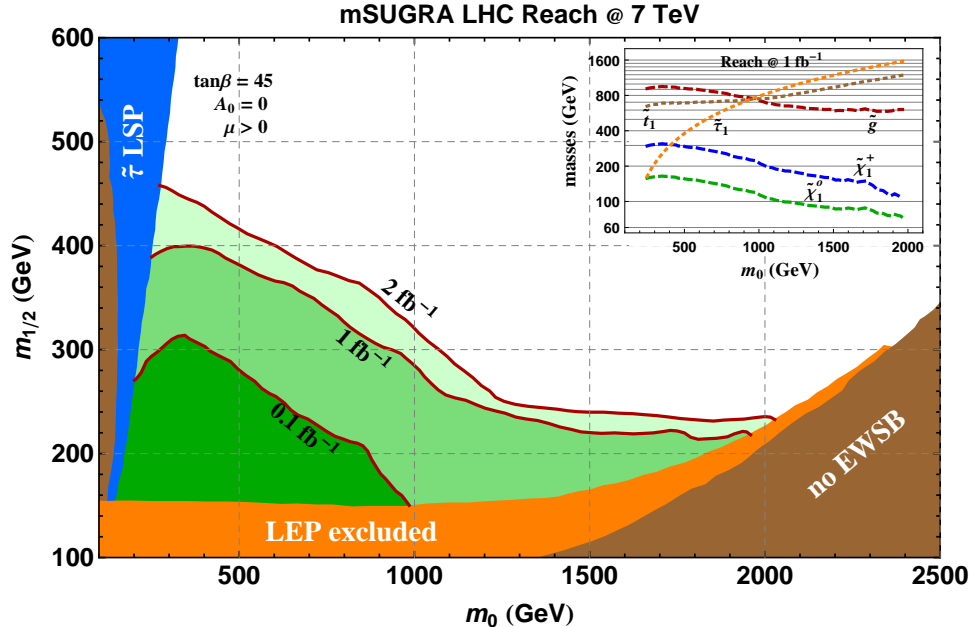


FIG. 4: A reach plot for mSUGRA using the signature analysis and the standard model backgrounds of this work given in Table (I) at the LHC with $\sqrt{s} = 7$ TeV and 1 fb^{-1} of integrated luminosity. The mSUGRA parameters used are $A_0 = 0$, $\tan\beta = 45$, $\text{sign}(\mu) = 1$. The analysis is done under the conditions of REWSB and the LEP and Tevatron constraints but without the imposition of the relic density and FCNC constraints. The condition used for a signal to be observable is $S > \max(5\sqrt{SM}, 10)$ where SM stands for the standard model background. Early LHC reaches at 1 fb^{-1} for the gluino (\tilde{g}), the chargino ($\tilde{\chi}_1^\pm$), the neutralino (χ_1^0), the stau ($\tilde{\tau}_1$), and the stop (\tilde{t}_1) are exhibited in the inset where the y axis is plotted on a logarithmic scale.

providing important cross-checks for the discovery of supersymmetry. In Fig. (5) we also exhibit discovery channels for 0.1 fb^{-1} , 1 fb^{-1} , and 2 fb^{-1} of data which shows the identities of the new signature channels that open as one increases the integrated luminosity. It is interesting to ask how the number of visible signatures depends on the integrated luminosity. An analysis of this issue is given in Fig. (6) where a plot is given of the number of signature channels where the SUSY signal becomes visible as a function of the integrated luminosity. The figure shows that the number of discovery channels increases rather sharply with luminosity and can become as large as 10 or more at 1 fb^{-1} of integrated luminosity. Quite interestingly the analysis of Fig. (6) also exhibits that a SUSY discovery can occur with an integrated luminosity as low as 0.1 fb^{-1} still with several available discovery channels.

As noted earlier all of the benchmarks listed in Table (III) are discoverable and further, as shown in Fig. (7), all of them are also consistent with the current limits on the spin independent neutralino-proton cross sections from CDMS-II and XENON-100 and can be seen in the next generation of xenon and germanium experiments. Finally in Table (IV) we exhibit the light sparticle spectrum for a subset of the benchmarks given in Table (III). Here we note that some of the models in Table (III), as, for example, the model C1, have typically a small value of μ indicating that they reside on or near the so-called hyperbolic branch/focus point region [46] of radiative breaking of the electroweak symmetry. Such models would have scalar masses which are typically heavier and often much heavier than the gaugino masses as can be seen in Table (IV).

V. MODEL SIMULATIONS

We give now a further discussion of the model simulations. As Fig. (5) indicates, the primary discovery channels for supersymmetry at $\sqrt{s} = 7$ TeV will be jet-based signatures which are designed to be as inclusive as possible to increase the number of signal events. This will need to take precedence over signal purity (i.e. efficiency to reject background) at values of integrated luminosity at or below 1 fb^{-1} . Four of the five chargino NLSP benchmarks can be discovered via jet-based signatures within the first 100 pb^{-1} of data, with the remainder (Chargino 2) reaching a

A Display of Visible Discovery Channels for 0.1 fb^{-1} , 1 fb^{-1} and 2 fb^{-1} at $\sqrt{s} = 7 \text{ TeV}$.

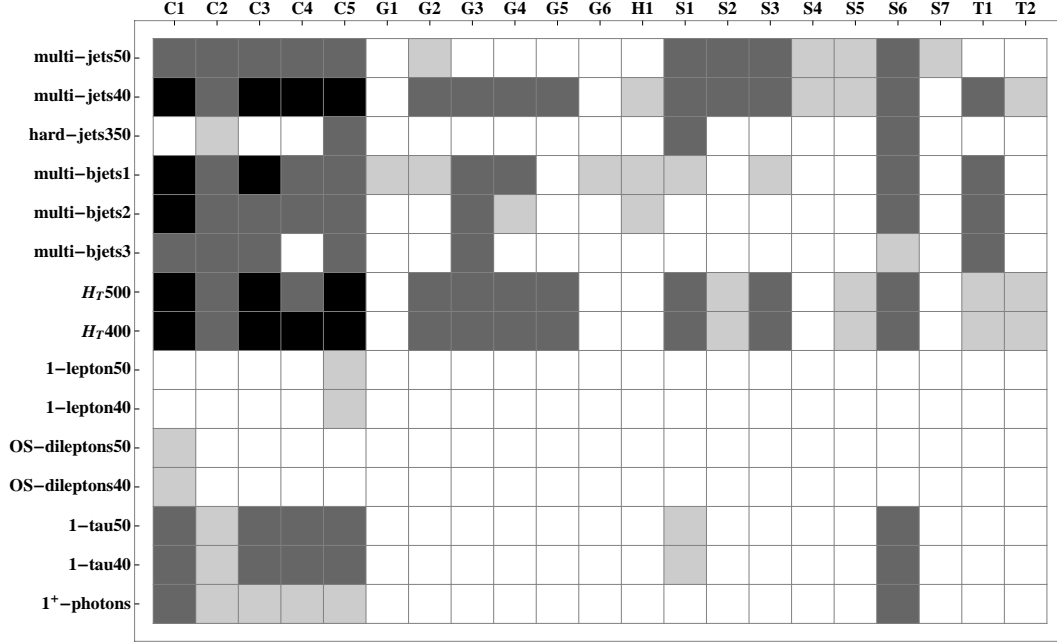


FIG. 5: An exhibition of the visible discovery channels for 0.1 fb^{-1} (black squares), 1 fb^{-1} (dark gray squares) and 2 fb^{-1} (light gray squares) at $\sqrt{s} = 7 \text{ TeV}$. The discovery channels are listed in Table II. Here we are using the convention that C denotes a chargino model, G denotes a gluino model, H denotes a Higgs model, S denotes a stau model, and T denotes a stop model.

A Display of the Number of Discovery Channels as a Function of Integrated Luminosity.

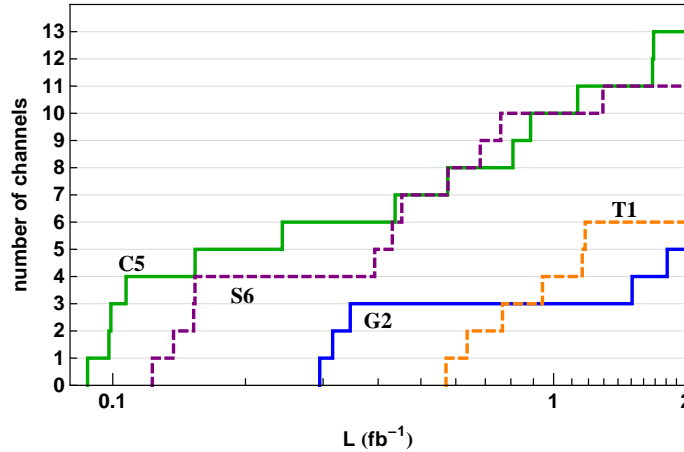


FIG. 6: An exhibition of the rapid rise in the number of discovery channels vs integrated luminosity for four early discovery benchmarks given in Table (III). The number of discovery channels for supersymmetry in each case is in excess of five and in some cases as large as 10 or above at 1 fb^{-1} of data at $\sqrt{s} = 7 \text{ TeV}$.

five-sigma significance in the multijets100 channel within 200 pb^{-1} . The stau NLSP models favor traditional multijet signatures such as multijets200 and H_T 500 which involve much harder jet- p_T requirements. Among our benchmarks the stau NLSP cases tend to have the heaviest gluinos with $709 \text{ GeV} \leq m_{\tilde{g}} \leq 912 \text{ GeV}$ and lightest squarks in the range of $330\text{-}600 \text{ GeV}$. These examples will therefore exhibit very similar characteristics in the early data taking, with the heavier gluino producing long cascades of moderately energetic jets which satisfy the high- p_T jet requirements common in analyses at $\sqrt{s} = 14 \text{ TeV}$. By contrast, our Higgs, stop, and gluino NLSP models favor discovery channels with much looser jet requirements to increase the signal size. These include the H_T 400, multi-bjets1 and multi-bjets2

A Display of Benchmarks as Dark Matter Candidates.

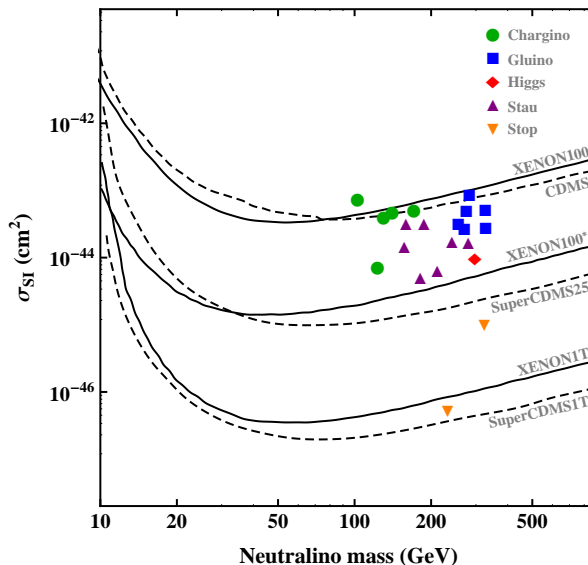


FIG. 7: An exhibition of the spin independent neutralino-proton cross section, σ_{SI} , for the benchmark models. These are labeled by the NLSP, which under the applied constraints allow chargino (green circles), stau (purple triangles), gluino (blue squares), CP odd Higgs (red diamond), and stop (orange inverted triangles) NLSPs. In the plot the curve labeled XENON100* is the expected sensitivity of XENON100 with $6000\text{kg} \times \text{days}$ of data, the curve labeled XENON1T is the expected sensitivity for $1\text{ton} \times \text{year}$ of data and the curves labeled SuperCDMS25 and SuperCDMS1T are the expected sensitivities for the two SuperCDMS experiments.

channels. We can understand the prevalence of b-jet signatures because of the rather small mass gaps between the lightest $SU(3)$ -charged state (i.e. the gluino or squark) and the LSP which eventually appears at the end of the cascade [47]. For example, the mass gap between the gluino and the LSP for the gluino NLSP models ranges from 60 to 160 GeV, with an average gluino mass for these models of 390 GeV. We note that these b-jet channels are defined with a requirement that $p_T^{\text{jet}} \geq 40$ GeV for the b-tagged jet and we impose a veto on isolated leptons (e and μ). The latter is not strictly necessary to achieve a high signal significance, but imposing the leptonic veto sufficiently reduced the SM background arising from the t, \bar{t} background samples to increase signal significance by a factor of about 65% on average.

The discussion above indicates an important concern for experimentalists facing the challenge of extracting the most signal possible from the first year of LHC data. Traditional signature definitions are often designed to enhance the signal-to-background purity so as to be able to make meaningful exclusive measurements of key quantities – often the edges or end points of various kinematic distributions. As we will see below, there will likely be few opportunities to employ these analysis techniques with only 1 fb^{-1} of data at $\sqrt{s} = 7$ TeV, even if we are fortunate enough to discover supersymmetry in multiple channels. It thus may make sense to seek, at the expense of purity, a more inclusive set of signature definitions. Consider, for example, the object defined by

$$\sum_{i=1}^4 p_{T_i} + \cancel{E}. \quad (4)$$

When the four objects entering (4) are restricted to the four hardest jets, the above is typically referred to as effective mass (M_{eff}), and has often been studied in the context of multijet channels for discovery of supersymmetry [48, 49]. When we wish to restrict our attention to jets only, we will refer to (4) as the “jet effective mass” of the event. A more inclusive definition is to allow the four hardest visible objects to enter (4) – in particular, hard leptons. For the sake of clarity, when we wish to consider this more expansive variable we will refer to it as “generalized effective mass” or H_T , as we did in Table II. In the case of this generalized effective mass we will also impose an overall collective cut on the scalar sum of all p_T ’s for these objects, as opposed to cuts on individual object p_T ’s. In an environment where jet- p_T measurements are likely to be less accurate than we might like, this is a reasonable variable to employ and we find it to be particularly effective across many of our benchmark categories. Similarly, we have given in Table (II) a number of variants to the jet- p_T requirements to give the reader the sense of how relaxing these requirements may

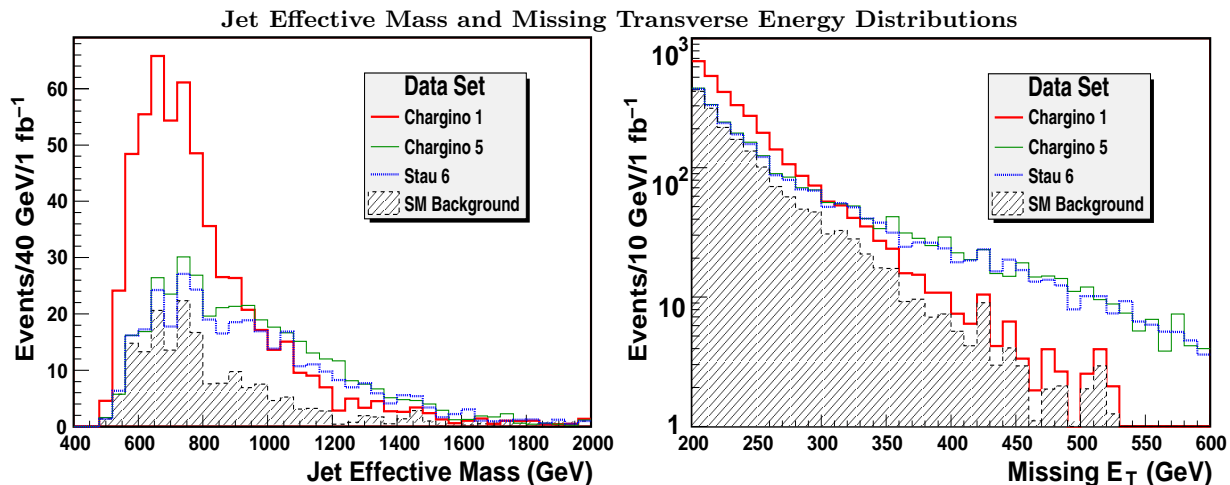


FIG. 8: Left: Effective mass distribution (multi-jets100) of the four hardest jets for three benchmark models with strong signals in this channel: Chargino 1 red (heavy) line, Chargino 5 green (thin) line and Stau 6 blue (dash-dotted) line. This signature is defined in Eq. (4) in the text. Signal curves are signal + SM background, with the background component indicated by the hatched region. Right: Missing transverse energy distribution for the same three models on a logarithmic scale. Again the SM component is indicated by the hatched region.

accelerate discovery. We will investigate this further with a few of our benchmarks below. In general, the lighter jet requirements tend to result in a signal which becomes significant sooner, but when both channels are significant the stronger jet case may often have the better signal-to-background figure.

We find very few discovery channels in the leptonic sector for our benchmark models. In the one-lepton plus jets channels at 1 fb^{-1} we find between 10 and 50 events for our chargino NLSP and stau NLSP models and less than 10 events for the Higgs, gluino and stop NLSP models. This is to be contrasted with 367 background events with the 40 GeV jet requirement (1-lepton40) and 350 with the stricter jet requirement (1-lepton100). These channels achieve five-sigma significance only for model Chargino 5, and only after 2 fb^{-1} of data. The opposite-sign (OS) dilepton channels give $\mathcal{O}(10)$ signal events after 1 fb^{-1} of data for our chargino NLSP models only. These cases just fail to reach five-sigma significance until 2 fb^{-1} of data. Event rates for same-sign dileptons and trileptons are consistent with zero for all benchmarks at 1 fb^{-1} , with a handful of events expected at 2 fb^{-1} . These “gold-plated” supersymmetry channels will need to wait for higher center of mass energies or larger data sets to make their presence manifest.

Finally, we make a few remarks about discovery channels with an imperfect detector. Early results from both detectors at the LHC seem to indicate that measurement of missing transverse energy appears to fit Monte Carlo predictions within reason and the overall error in determining missing E_T is less severe than many pessimists had feared [50]. This is welcome news, as our benchmarks will all require missing E_T as part of any search strategy. None of the benchmarks we studied are visible above backgrounds without this important ingredient, with the number of signal events becoming comparable to the SM background only when $\cancel{E}_T \geq 200 \text{ GeV}$ or higher is employed. We also point out that many of our best signals involve tagged b jets. As mentioned previously, we updated the PGS4 b tagging to reflect the more optimistic expectations of the ATLAS and CMS collaborations. Achieving these efficiency targets early in LHC data taking will be important for many supersymmetric models relevant to the LHC at $\sqrt{s} = 7 \text{ TeV}$.

To understand these features we will look a bit more closely at eight of our benchmarks from Table (III) chosen to represent an array of phenomenologies at the LHC. These eight benchmarks are collected in Table (IV) where we provide physical masses of some of the key superpartners relevant for LHC signatures. For each benchmark we give in Table (V) the number of signal events in 1 fb^{-1} for a selection of signatures from Table (II), as well as the standard model background count and the signal significance. In this table we have included, for illustrative purposes, a modification of the multi-jet signature in which we merely require at least four jets, each with $p_T^{\text{jet}} \geq 40 \text{ GeV}$ in addition to the missing transverse energy and transverse sphericity cut. The table illustrates the relative paucity of leptonic signatures across all of our benchmark models and the importance of employing relative loose jet- p_T requirements in multijet signatures.

In the left panel of Fig. (8) we exhibit the multijets100 signature, defined by Eq. (4), for the three benchmarks of Table (V) with the strongest signal. The distribution of m_{eff} for the three models is given in terms of the signal plus the SM background, normalized to 1 fb^{-1} , with the SM background also shown separately in the hatched region. The strongest signal comes from Chargino 1 whose overall distribution is very similar in size and shape to that of

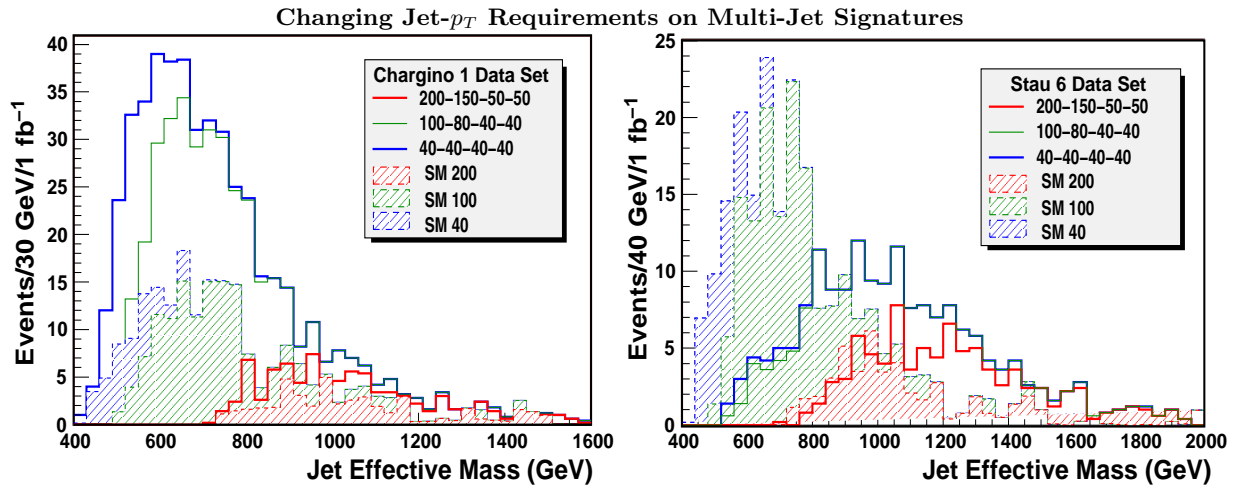


FIG. 9: The effect of changing the minimum transverse momentum of leading jets for multijet signatures is exhibited for two models: Chargino 1 (left panel) and Stau 6 (right panel). Heavy (red line) distributions represent the strict multijets200 signature, thin (green line) distributions are the softer multijets100 signature, and medium (blue line) distributions are for the multijets40 signature. The legend gives the minimum p_T^{jet} requirement for the four hardest jets in the event. In this figure we show the signal superimposed on the SM background separately to distinguish between the three cases.

the SM background, while Chargino 5 and Stau 6 peak at slightly larger values. These distributions are heavily influenced by the distributions in \cancel{E}_T , which are plotted on a logarithmic scale in the right panel of Fig. (8). We can understand these shapes from the values in Table (IV): the relatively light gluino of model Chargino 1 is the lightest $SU(3)$ -charged state which will decay to low- p_T jets, while the lightest such state in the other two cases is the stop which has a slightly higher mass ($m_{\tilde{t}} = 402$ GeV for Chargino 5 and 497 GeV for Stau 6). For these two cases the dominant supersymmetric production processes involve the associated production of a gluino and a squark, with the decay of the gluino to on-shell squarks producing slightly harder jets. An examination of the multijet m_{eff} variable with varying jet requirements should reveal the general mass scale for the low-lying strongly coupled superpartners, and this information should assist in optimizing jet- p_T requirements on signals with lower statistics.

In Fig. (9) we investigate the effect of changing these jet- p_T requirements for Chargino 1 (left panel) and Stau 6 (right panel). Here we include the signatures denoted multi-jets200 and multi-jets100 in Table (II) as well as our softer signature multi-jets40 from Table (V). In this case we show the signal superimposed on the SM background separately to distinguish among the three cases. Loosening the jet requirements populates the lower energy bins in m_{eff} for both the signal and the background, leaving the higher energy bins mostly unaffected. Therefore these softer cuts tend to boost the signal significance of models such as Chargino 1 with softer jets, while actually reducing the significance of models like Stau 6 where jets carry much more p_T on average. This is also reflected in the signal significances at 1 fb^{-1} in Table (V). For these models all three signature definitions yield a discovery, but for other models such as Gluino 2 the softer jet requirement is crucial to making an early discovery. In Fig. (10) we plot the generalized H_T 400 variable for the three models for which this is the leading discovery channel: Chargino 5, Stau 6, and Gluino 2. For the last case, this channel produces a discovery in approximately 300 pb^{-1} while other channels must wait for more data for a five-sigma excess. Despite the very light gluino in model Gluino 2, the compressed spectrum of this model produces extremely soft jets and a relatively low jet multiplicity for gluino pair production events. Expanding the definition to include all visible decay products produces a stronger signal.

As mentioned above, the peak in the jet effective mass distribution – or the energy at which the signal begins to exceed the SM background – is a relatively good indicator of the rough mass scale of the lightest $SU(3)$ -charged superpartner [49]. Apart from this rough estimate, one might ask if there are other properties of the superpartner spectrum that can be “measured,” even at such low statistics. We believe that the answer is in principle yes, depending on the model. The most well-known measurement technique is to form the invariant mass of opposite-sign dilepton pairs and look for an edge, or end point, in the distribution. This procedure is often performed after a flavor subtraction is done (i.e., the combination $e^+e^- + \mu^+\mu^- - e^+\mu^- - e^-\mu^+$ is formed) to reduce SM and SUSY combinatorial backgrounds. After 1 fb^{-1} there is unlikely to be sufficient numbers of OS dilepton events to perform this subtraction, or even to identify a true edge. Even after 2 fb^{-1} the statistics are sufficiently low to make this measurement difficult in all but the most favorable model points. We illustrate this in Fig. (11), normalized to 2 fb^{-1} of data. It is tempting to see an edge in the invariant mass distribution for Chargino 1 (see inset for a clear view).

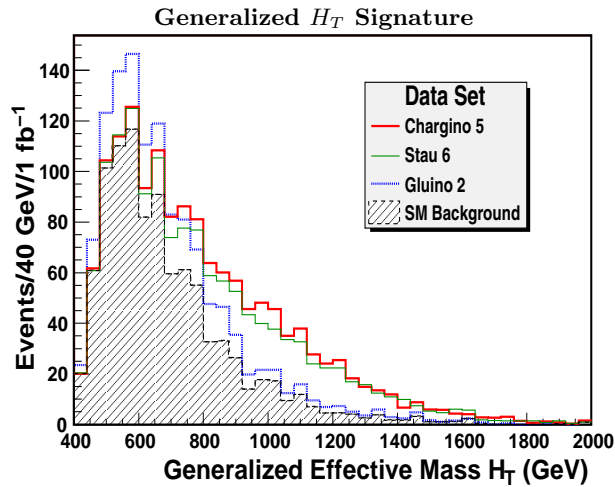


FIG. 10: Distribution of H_T , defined by Eq. (4) but applied to the hardest four visible objects in the event as opposed to the four hardest jets with an isolated lepton veto. The signal plus background distribution is given for the three benchmarks for which this was the best discovery channel: Chargino 5 heavy (red) line, Stau 6 thin (green) line and Gluino 2 medium (blue) line. The component of the distribution made up of SM background events is indicated by the hatched region.

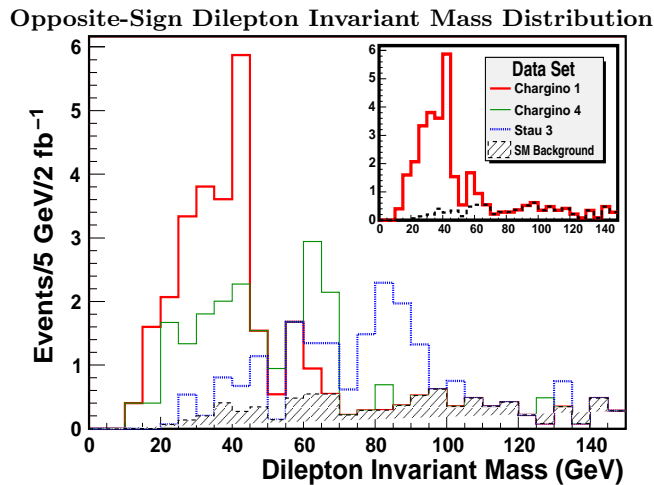


FIG. 11: The opposite-sign dilepton invariant mass is displayed for events satisfying the signature definitions denoted OS-dileptons40 in Table (II). The models shown are Chargino 1 heavy (red) line, Chargino 4 thin (green) line and Stau 3 medium (blue) line. As with previous distributions the curves are for the signal + SM background, with the background component indicated by the hatched region. The inset shows the distribution for Chargino 1 alone, to exhibit the edge at approximately 50 GeV.

But the low statistics are evidenced by the scale on the vertical axis. The sharpness of the edge is largely an artifact of simulating our signal sets at the 5 fb^{-1} level and then rescaling to a smaller integrated luminosity. Nevertheless, this edge is indeed real and accurately describes the mass distribution between the lightest and second-lightest neutralino. The first hint of the “spoiler mode” $\chi_2^0 \rightarrow Z \chi_1^0$ present in the Stau 3 benchmark is also present in Fig. (11).

Potentially more promising are measurements based on the invariant mass distribution of events with precisely two b-tagged jets. In Fig. (12) we give di-bjet invariant mass distributions for four models with particularly strong signals in this channel. In the right panel we give two models for which the b-jet channels are the strongest discovery modes, Gluino 3 and Stop1, and with a sufficient amount of data it should be able to measure the mass difference between the gluino and the lightest neutralino.

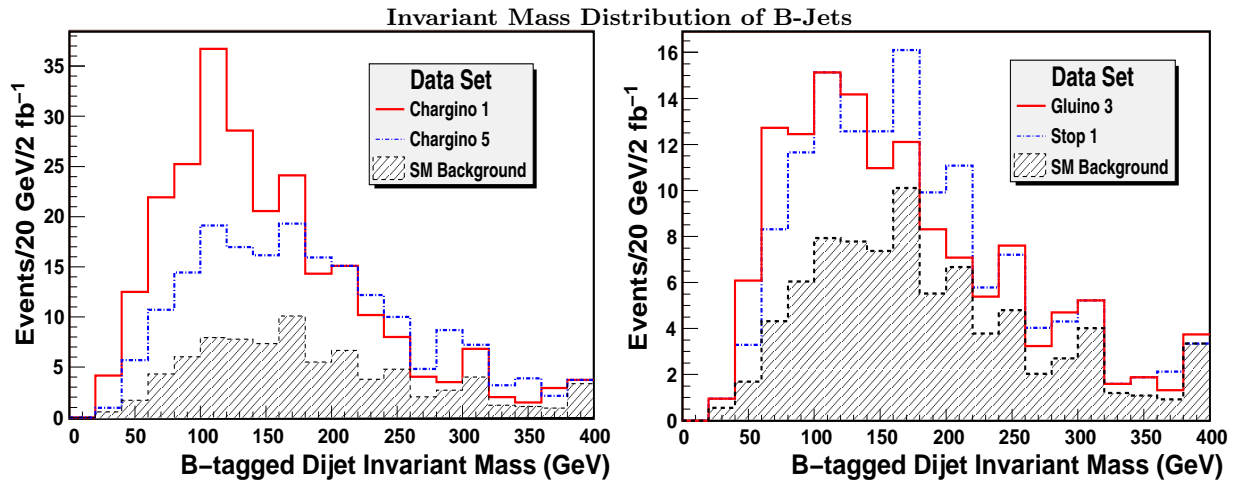


FIG. 12: The invariant mass distribution of b-jet pairs for events with precisely two b-tagged jets, each with $p_T^{\text{jet}} \geq 40$ GeV, is given for events which satisfy our initial cuts of transverse sphericity $S_T \geq 0.2$ and at least 200 GeV of \cancel{E}_T . No lepton veto is imposed on these distributions. As with previous distributions the curves are for signal + SM background, with the background component indicated by the hatched region. Left panel: Chargino 1 heavy (red) line and Chargino 5 dash-dotted (blue) line. Right panel: Gluino 3 heavy (red) line and Stop 1 dash-dotted (blue) line.

VI. CONCLUSIONS

We have given here an analysis of the potential of the LHC in early runs at $\sqrt{s} = 7$ TeV to discover supersymmetry with 1 fb^{-1} of data. We have carried out an independent analysis of the standard model backgrounds at $\sqrt{s} = 7$ TeV and 1 fb^{-1} of integrated luminosity which are generally consistent with a previous study [4]. Our analysis is done within the framework of the MSSM. However, the parameter space for soft breaking for the MSSM is rather large (with over a hundred parameters) and thus intractable. This parameter space is significantly reduced in the models we consider. Thus in the analysis of this work we use the framework of mSUGRA which has four parameters and the sign of μ , as well as supergravity models with nonuniversality in the gaugino sector which increases the number of parameters to six and the sign of μ . The analysis is done under the imposition of theoretical constraints which include the radiative breaking of the electroweak symmetry, R parity conservation, and conservation of charge and color, as well as under the experimental constraints which include constraints on the relic density from WMAP, constraints from flavor changing neutral currents, and the experimental lower limit constraints on the masses of the Higgs bosons and on the sparticle masses. The residual model space which passes both the theoretical and the experimental constraints as described above is still large and we use a selection criteria in its further exploration. Noting that the central theme of the analysis is the discovery of supersymmetry in early runs, our search for models is then narrowed to such models as are discoverable with $\sqrt{s} = 7$ TeV and $1\text{-}2 \text{ fb}^{-1}$ of data. Within this general theme we choose the models as broadly as possible to encompass as many diverse possibilities as possible. Specifically we select models so that all allowed NLSPs such as the chargino, the stau, the gluino, the CP odd Higgs, and the stop are included. Using the above criteria we have presented a set of benchmarks for early discovery in Table (III). We observe that in Table (III) all the NLSPs mentioned above are represented. Further, in Table (III) the range of inputs varies widely. Thus, for example, m_0 ranges from 101 to 2225, $m_{1/2}$ ranges from 313 to 755, A_0 ranges from -2531 to 2710 (all masses in GeV), and $\tan\beta$ ranges from 5.7 to 47.2. The analysis of this work shows that an $m_{1/2}$ mass up to 400 GeV and m_0 up to 2 TeV could be accessible for certain combinations of soft parameters. Further, the precise set of discovery modes in which the benchmarks will become visible are identified. It is shown that most of the benchmarks have at least a minimum of five discovery channels and several of them have as many as 10 in which the SUSY signal is discoverable. We have also exhibited the dependence of the number of discovery channels as a function of the integrated luminosity which shows its rapid increase as the integrated luminosity increases toward 1 fb^{-1} for the set of discoverable models investigated. Thus if SUSY is found in one of the signature channels for any of the benchmarks given in Table (III), then it should also show up in other signature channels as identified in Fig. (5) providing important cross-checks for the discovery of supersymmetry. All the benchmarks exhibited are consistent with the current limits on the spin independent neutralino-proton cross section from XENON100 and CDMS-II dark matter detectors. Further, all of the benchmarks will be accessible in the next generation of dark matter experiments.

Acknowledgments: Communications with Johan Alwall and Timothy Stelzer regarding MadGraph and with Andre Lessa regarding the analysis of [4] are acknowledged. This research is supported in part by NSF Grants No. PHY-0653587 and No. PHY-0757959.

VII. TABLES

A display of signatures/cuts used in early discovery analysis at the LHC at $\sqrt{s} = 7$ TeV

	Signature Name	Description of Cut	
1	monojets	$n(\ell) = 0$	$p_T(j_1) \geq 100$ GeV, $p_T(j_2) < 20$ GeV
2	multi-jets200	$n(\ell) = 0$	$p_T(j_1) \geq 200$ GeV, $p_T(j_2) \geq 150$ GeV, $p_T(j_4) \geq 50$ GeV
3	multi-jets100	$n(\ell) = 0$	$p_T(j_1) \geq 100$ GeV, $p_T(j_2) \geq 80$ GeV, $p_T(j_4) \geq 40$ GeV
4	hard-jets500	$n(\ell) = 0$	$p_T(j_2) \geq 500$ GeV
5	hard-jets350	$n(\ell) = 0$	$p_T(j_2) \geq 350$ GeV
6	multi-bjets1	$n(\ell) = 0, n(b) \geq 1$	
7	multi-bjets2	$n(\ell) = 0, n(b) \geq 2$	
8	multi-bjets3	$n(\ell) = 0, n(b) \geq 3$	
9	H_T 500	$n(\ell) + n(j) \geq 4$	$p_T(1) \geq 100$ GeV, $\sum_{i=1}^4 p_T(i) + \cancel{E}_T \geq 500$ GeV
10	H_T 400	$n(\ell) + n(j) \geq 4$	$p_T(1) \geq 100$ GeV, $\sum_{i=1}^4 p_T(i) + \cancel{E}_T \geq 400$ GeV
11	1-lepton100	$n(\ell) = 1$	$p_T(\ell_1) \geq 20$ GeV, $p_T(j_1) \geq 100$ GeV, $p_T(j_2) \geq 50$ GeV
12	1-lepton40	$n(\ell) = 1$	$p_T(\ell_1) \geq 20$ GeV, $p_T(j_2) \geq 40$ GeV
13	OS-dileptons100	$n(\ell^+) = n(\ell^-) = 1$	$p_T(\ell_2) \geq 20$ GeV, $p_T(j_1) \geq 100$ GeV, $p_T(j_2) \geq 50$ GeV
14	OS-dileptons40	$n(\ell^+) = n(\ell^-) = 1$	$p_T(\ell_2) \geq 20$ GeV, $p_T(j_2) \geq 40$ GeV
15	SS-dileptons100	$n(\ell^+ \ell^-) = n(\ell) = 2$	$p_T(\ell_2) \geq 20$ GeV, $p_T(j_1) \geq 100$ GeV, $p_T(j_2) \geq 50$ GeV
16	SS-dileptons40	$n(\ell^+ \ell^-) = n(\ell) = 2$	$p_T(\ell_2) \geq 20$ GeV, $p_T(j_2) \geq 40$ GeV
17	3-leptons100	$n(\ell) = 3$	$p_T(\ell_3) \geq 20$ GeV, $p_T(j_1) \geq 100$ GeV, $p_T(j_2) \geq 50$ GeV
18	3-leptons40	$n(\ell) = 3$	$p_T(\ell_3) \geq 20$ GeV, $p_T(j_2) \geq 40$ GeV
19	4 ⁺ -leptons	$n(\ell) \geq 4$	$p_T(\ell_4) \geq 20$ GeV, $p_T(j_2) \geq 40$ GeV
20	1-tau100	$n(\tau) = 1$	$p_T(\tau_1) \geq 20$ GeV, $p_T(j_1) \geq 100$ GeV, $p_T(j_2) \geq 50$ GeV
21	1-tau40	$n(\tau) = 1$	$p_T(\tau_1) \geq 20$ GeV, $p_T(j_2) \geq 40$ GeV
22	OS-ditau100	$n(\tau^+) = n(\tau^-) = 1$	$p_T(\tau_2) \geq 20$ GeV, $p_T(j_1) \geq 100$ GeV, $p_T(j_2) \geq 50$ GeV
23	OS-ditau40	$n(\tau^+) = n(\tau^-) = 1$	$p_T(\tau_2) \geq 20$ GeV, $p_T(j_2) \geq 40$ GeV
24	SS-ditau100	$n(\tau^+ \tau^-) = n(\tau) = 2$	$p_T(\tau_2) \geq 20$ GeV, $p_T(j_1) \geq 100$ GeV, $p_T(j_2) \geq 50$ GeV
25	SS-ditau40	$n(\tau^+ \tau^-) = n(\tau) = 2$	$p_T(\tau_2) \geq 20$ GeV, $p_T(j_2) \geq 40$ GeV
26	3 ⁺ -taus100	$n(\tau) \geq 3$	$p_T(\tau_3) \geq 20$ GeV, $p_T(j_1) \geq 100$ GeV, $p_T(j_2) \geq 50$ GeV
27	3 ⁺ -taus40	$n(\tau) \geq 3$	$p_T(\tau_4) \geq 20$ GeV, $p_T(j_2) \geq 40$ GeV
28	1 ⁺ -photon	$n(\gamma) \geq 1$	$p_T(j_2) \geq 40$ GeV

TABLE II: List of signatures and cuts used in the early discovery analysis. Our notation is as follows: $\ell = e, \mu$, $n(x)$ is the number of object x in the event, and $p_T(x_n)$ is the transverse momentum of the n^{th} hardest object x . For the case of $p_T(\tau)$ we take this to mean the visible part of the p_T from a hadronically decaying tau. We required $\cancel{E}_T \geq 200$ GeV and a minimum transverse sphericity of 0.2. The symbol $|$ should be read as the logic ‘‘or’’: i.e. the cut $n(\tau^+ | \tau^-) = 2$ would be read ‘‘the number of τ^+ equals 2 or the number of τ^- equals 2.’’

Benchmarks for Early Discovery at $\sqrt{s} = 7$ TeV with 2 fb^{-1}

Label	NLSP	m_0	$m_{\frac{1}{2}}$	A_0	$\tan\beta$	δ_2	δ_3	σ_{SUSY} (pb)	σ_{SI} (10^{-44} cm^2)
C1	χ_1^\pm	1663	309	1508	32.9	0.553	-0.687	24.3	7.0
C2	χ_1^\pm	449	330	176	20.3	-0.382	-0.151	2.4	3.7
C3	χ_1^\pm	1461	361	1327	30.3	-0.241	-0.702	14.8	4.5
C4	χ_1^\pm	1264	445	1775	24.7	0.718	-0.736	11.3	4.7
C5	χ_1^\pm	240	313	-522	5.48	-0.376	-0.106	3.5	0.7
G1	\tilde{g}	1694	755	-2128	45.7	0.745	-0.803	2.2	4.9
G2	\tilde{g}	2231	639	2710	18.0	0.543	-0.850	24.2	3.0
G3	\tilde{g}	2276	615	-2407	47.2	0.631	-0.784	3.1	2.6
G4	\tilde{g}	2180	651	-2271	47.1	0.680	-0.817	5.8	8.3
G5	\tilde{g}	2126	683	2924	38.0	0.580	-0.849	19.4	4.8
G6	\tilde{g}	1983	749	-2332	46.3	0.562	-0.824	3.7	2.7
H1	A^o	2225	674	-2531	47.3	0.783	-0.703	0.3	0.9
S1	$\tilde{\tau}_1$	117	394	0	15.9	-0.327	-0.177	1.4	1.4
S2	$\tilde{\tau}_1$	101	446	-153	6.1	0.607	-0.207	0.4	0.5
S3	$\tilde{\tau}_1$	102	470	183	15.3	0.603	-0.266	0.5	3.0
S4	$\tilde{\tau}_1$	309	581	-613	27.7	0.839	-0.400	0.6	1.6
S5	$\tilde{\tau}_1$	135	688	-184	5.7	-0.052	-0.499	0.4	1.6
S6	$\tilde{\tau}_1$	114	404	27	13.0	-0.369	-0.267	2.0	3.0
S7	$\tilde{\tau}_1$	114	518	87	10.4	0.266	-0.247	0.2	0.6
T1	\tilde{t}_1	1726	548	4197	21.2	0.132	-0.645	2.3	5.0×10^{-3}
T2	\tilde{t}_1	1590	755	3477	23.4	0.805	-0.803	3.8	9.4×10^{-2}

TABLE III: Benchmarks for *models discoverable* at the LHC at $\sqrt{s} = 7$ TeV with 2 fb^{-1} of integrated luminosity. The model inputs are given at $M_{GUT} = 2 \times 10^{16}$ GeV, $\text{sign}(\mu) = +1$, and $\delta_1 = 0$. The displayed masses are in GeV. All models satisfy REWSB and the experimental constraints as discussed in Sec. (II). The spin independent direct detection cross section, σ_{SI} , is exhibited as well as the cross section σ_{SUSY} for the production of supersymmetric particles at $\sqrt{s} = 7$ TeV. Our analysis shows that all the models listed in this table are discoverable at the 5σ level above the background in *several channels* as exhibited in Fig. (5).

Sparticle mass spectra for the benchmarks

Label	C1	C2	C3	C4	C5	G1	G2	G3	G4	G5	G6
NLSP	χ_1^\pm	χ_1^\pm	χ_1^\pm	χ_1^\pm	χ_1^\pm	\tilde{g}	\tilde{g}	\tilde{g}	\tilde{g}	\tilde{g}	\tilde{g}
σ_{SUSY} (pb)	24.3	2.4	14.8	11.3	3.5	2.2	24.2	3.1	5.8	19.4	3.7
μ	145	345	239	231	489	480	314	523	434	324	539
$m_{\tilde{N}_1}$	103	130	140	171	123	327	256	270	283	275	328
$m_{\tilde{N}_2}$	157	151	189	240	146	485	324	522	439	333	541
$m_{\tilde{C}_1^\pm}$	141	150	183	229	145	480	316	520	435	326	539
$m_{\tilde{\tau}_1}$	1463	441	1318	1170	260	1079	2155	1542	1475	1719	1311
$m_{\tilde{t}_1}$	922	560	828	621	402	612	1145	1115	1048	1054	863
$m_{\tilde{g}}$	316	698	341	354	680	452	314	432	393	325	421

Label	H1	S1	S2	S3	S4	S5	S6	S7	T1	T2
NLSP	A^o	$\tilde{\tau}_1$	$\tilde{\tau}_1$	$\tilde{\tau}_1$	$\tilde{\tau}_1$	$\tilde{\tau}_1$	$\tilde{\tau}_1$	$\tilde{\tau}_1$	\tilde{t}_1	\tilde{t}_1
σ_{SUSY} (pb)	0.3	1.4	0.4	0.5	0.6	0.4	2.0	0.2	2.3	3.8
μ	630	425	426	301	393	443	388	432	1213	691
$m_{\tilde{N}_1}$	297	157	181	188	241	280	159	211	232	324
$m_{\tilde{N}_2}$	630	198	408	303	395	415	189	408	508	689
$m_{\tilde{C}_1^\pm}$	629	198	405	295	390	409	187	406	508	687
$m_{\tilde{\tau}_1}$	1456	167	194	192	248	289	176	221	1546	1436
$m_{\tilde{t}_1}$	1032	541	504	529	329	506	497	615	258	357
$m_{\tilde{g}}$	594	771	835	817	834	817	709	913	532	422

TABLE IV: An exhibition of the light sparticles for the benchmarks given. These benchmarks are listed in Table (III). All masses are given in GeV.

LHC discovery channels after 1 fb^{-1} of integrated luminosity

Signature Name		SM	C1	C4	C5	G2	G3	S3	S6	T1
Multi-jets200	Events	47	91	68	105	28	16	49	88	12
	S/\sqrt{B}	...	13.3	9.9	15.2	4.1	2.4	7.2	12.7	1.8
Multi-jets100	Events	180	401	225	213	114	83	77	171	69
	S/\sqrt{B}	...	29.9	16.8	15.9	8.5	6.2	5.8	12.8	5.2
Multi-jets40	Events	215	497	316	218	135	107	77	176	85
	S/\sqrt{B}	...	33.9	21.6	14.9	9.2	7.3	5.3	12.0	5.8
H_T400	Events	965	1035	501	496	286	183	156	419	143
	S/\sqrt{B}	...	33.3	16.1	16.0	9.2	5.9	5.0	13.5	4.6
Multi-bjets1	Events	188	460	188	175	51	126	50	102	86
	S/\sqrt{B}	...	33.5	13.7	12.8	3.7	9.2	3.6	7.5	6.3
Multi-bjets2	Events	46	157	49	69	7	57	19	39	45
	S/\sqrt{B}	...	23.1	7.3	10.1	...	8.4	2.8	5.7	6.6
1-lepton40	Events	367	45	20	74	0	0	30	38	27
	S/\sqrt{B}	...	2.4	1.0	3.9	1.6	2.0	1.4

TABLE V: LHC discovery channels after 1 fb^{-1} of integrated luminosity for selected benchmark models from Table (IV). All signatures require transverse sphericity $S_T \geq 0.2$ and at least 200 GeV of \cancel{E}_T . For each signature the number of signal events is given, as well as the signal significance if there are sufficient signal events. We have also included a much weaker multijet signature (multijets40) in which the four jets are all required merely to satisfy $p_T^{\text{jet}} \geq 40$ GeV. This signature also appears in Fig. (9).

-
- [1] P. Nath, B. D. Nelson *et al.*, “The Hunt for New Physics at the Large Hadron Collider,” Nucl. Phys. Proc. Suppl. **200-202**, 185 (2010) [arXiv:1001.2693 [hep-ph]].
- [2] N. Bhattacharyya, A. Datta, S. Poddar, Phys. Rev. **D82**, 035003 (2010). [arXiv:1005.2673 [hep-ph]].
- [3] C. W. Bauer, Z. Ligeti, M. Schmaltz, J. Thaler and D. G. E. Walker, Phys. Lett. B **690**, 280 (2010) [arXiv:0909.5213 [hep-ph]].
- [4] H. Baer, V. Barger, A. Lessa and X. Tata, JHEP **1006** (2010) 102 [arXiv:1004.3594 [hep-ph]].
- [5] D. S. M. Alves, E. Izaguirre and J. G. Wacker, arXiv:1008.0407 [hep-ph].
- [6] K. Desch, H. K. Dreiner, S. Fleischmann, S. Grab and P. Wienemann, arXiv:1008.1580 [hep-ph].
- [7] J. Edsjo, E. Lundstrom, S. Rydbeck and J. Sjolín, JHEP **1003**, 054 (2010) [arXiv:0910.1106 [hep-ph]].
- [8] H. K. Dreiner, M. Kramer, J. M. Lindert and B. O’Leary, JHEP **1004**, 109 (2010) [arXiv:1003.2648 [hep-ph]].
- [9] J. Hubisz, J. Lykken, M. Pierini and M. Spiropulu, Phys. Rev. D **78**, 075008 (2008) [arXiv:0805.2398 [hep-ph]].
- [10] H. Baer, A. Lessa and H. Summy, Phys. Lett. B **674**, 49 (2009) [arXiv:0809.4719 [hep-ph]].
- [11] J. Dietrich [ATLAS Collaboration], arXiv:1005.2034 [hep-ex].
- [12] J. Alwall *et al.*, JHEP **0709**, 028 (2007) [arXiv:0706.2334 [hep-ph]].
- [13] T. Sjostrand, S. Mrenna and P. Z. Skands, JHEP **0605**, 026 (2006) [arXiv:hep-ph/0603175].
- [14] P. Skands *et al.*, JHEP **0407**, 036 (2004); PGS 4, J. Conway *et al.*
- [15] J. Alwall *et al.*, Eur. Phys. J. C **53**, 473 (2008) [arXiv:0706.2569 [hep-ph]].
- [16] M. L. Mangano, M. Moretti, F. Piccinini, R. Pittau and A. D. Polosa, JHEP **0307**, 001 (2003) [arXiv:hep-ph/0206293].
- [17] J. Pumplin, D. R. Stump, J. Huston, H. L. Lai, P. M. Nadolsky and W. K. Tung, JHEP **0207**, 012 (2002) [arXiv:hep-ph/0201195].
- [18] G.L. Bayatian *et al.* (CMS Collaboration). “CMS technical design report, volume I: Detector performance and software.”
- [19] G. Aad *et al.* [The ATLAS Collaboration], arXiv:0901.0512 [hep-ex].
- [20] A. H. Chamseddine, R. Arnowitt and P. Nath, Phys. Rev. Lett. **49** (1982) 970; P. Nath, R. L. Arnowitt and A. H. Chamseddine, Nucl. Phys. B **227**, 121 (1983); L. Hall, J. Lykken and S. Weinberg, Phys. Rev. **D27**, 2359 (1983).
- [21] A. Corsetti and P. Nath, Phys. Rev. D **64**, 125010 (2001); U. Chattopadhyay and P. Nath, Phys. Rev. D **65**, 075009 (2002); G. L. Kane, J. D. Lykken, S. Mrenna, B. D. Nelson, L. T. Wang and T. T. Wang, Phys. Rev. D **67**, 045008 (2003); A. Birkedal-Hansen and B. D. Nelson, Phys. Rev. D **67**, 095006 (2003); D. G. Cerdeno and C. Munoz, JHEP **0410**, 015 (2004); H. Baer, A. Mustafayev, S. Profumo, A. Belyaev and X. Tata, JHEP **0507**, 065 (2005); S. F. King, J. P. Roberts and D. P. Roy, JHEP **0710**, 106 (2007).
- [22] A. Birkedal-Hansen and B. D. Nelson, Phys. Rev. D **64**, 015008 (2001).
- [23] D. Feldman, Z. Liu and P. Nath, Phys. Lett. B **662**, 190 (2008); H. Baer, A. Mustafayev, E. K. Park and X. Tata, JHEP **0805**, 058 (2008); D. Feldman, Z. Liu and P. Nath, JHEP **0804**, 054 (2008); B. Altunkaynak, M. Holmes and B. D. Nelson, JHEP **0810**, 013 (2008); S. P. Martin, Phys. Rev. D **78** (2008) 055019; S. Bhattacharya, A. Datta and B. Mukhopadhyaya, Phys. Rev. D **78**, 115018 (2008); C. F. Berger, J. S. Gainer, J. L. Hewett and T. G. Rizzo, JHEP **0902**, 023 (2009).
- [24] K. Choi and H. P. Nilles, JHEP **0704**, 006 (2007) [arXiv:hep-ph/0702146].
- [25] B. Altunkaynak, P. Grajek, M. Holmes, G. Kane and B. D. Nelson, JHEP **0904**, 114 (2009) [arXiv:0901.1145 [hep-ph]]; B. Altunkaynak, B. D. Nelson, L. L. Everett, I. W. Kim and Y. Rao, JHEP **1005**, 054 (2010) [arXiv:1001.5261 [hep-ph]]; M. Holmes and B. D. Nelson, JCAP **0907**, 019 (2009) [arXiv:0905.0674 [hep-ph]].
- [26] D. Feldman, G. Kane, R. Lu and B. D. Nelson, Phys. Lett. B **687**, 363 (2010) [arXiv:1002.2430 [hep-ph]].
- [27] D. Feldman, Z. Liu, P. Nath and G. Peim, Phys. Rev. D **81**, 095017 (2010) [arXiv:1004.0649 [hep-ph]]; P. Konar, K. T. Matchev, M. Park and G. K. Sarangi, arXiv:1008.2483 [hep-ph]; I. Gogoladze, R. Khalid, S. Raza and Q. Shafi, arXiv:1008.2765 [hep-ph].
- [28] N. Jarosik *et al.*, arXiv:1001.4744 [astro-ph.CO].
- [29] G. W. Bennett *et al.* [Muon g-2 Collaboration], Phys. Rev. Lett. **92**, 161802 (2004) [arXiv:hep-ex/0401008].
- [30] M. Davier, A. Hoecker, B. Malaescu *et al.*, Eur. Phys. J. **C66**, 1-9 (2010). [arXiv:0908.4300 [hep-ph]].
- [31] T. C. Yuan, R. L. Arnowitt, A. H. Chamseddine and P. Nath, Z. Phys. C **26**, 407 (1984); D. A. Kosower, L. M. Krauss and N. Sakai, Phys. Lett. B **133**, 305 (1983); J. L. Lopez, D. V. Nanopoulos and X. Wang, Phys. Rev. D **49**, 366 (1994); U. Chattopadhyay and P. Nath, Phys. Rev. Lett. **86**, 5854 (2001).
- [32] T. Aaltonen *et al.* [CDF Collaboration], Phys. Rev. Lett. **100**, 101802 (2008) [arXiv:0712.1708 [hep-ex]].
- [33] C. Amsler *et al.* [Particle Data Group], Phys. Lett. B **667**, 1 (2008).
- [34] E. Barberio *et al.* [Heavy Flavor Averaging Group], arXiv:0808.1297 [hep-ex].
- [35] M. Misiak *et al.*, Phys. Rev. Lett. **98**, 022002 (2007) [arXiv:hep-ph/0609232].
- [36] G. Degrassi, P. Gambino and G. F. Giudice, JHEP **0012** (2000) 009; F. Borzumati, C. Greub, T. Hurth and D. Wyler, Phys. Rev. D **62**, 075005 (2000); M. E. Gomez, T. Ibrahim, P. Nath and S. Skadhauge, Phys. Rev. D **74** (2006) 015015.
- [37] N. Chen, D. Feldman, Z. Liu and P. Nath, Phys. Lett. B **685**, 174 (2010) [arXiv:0911.0217 [hep-ph]].
- [38] A. Djouadi, M. Drees and J. L. Kneur, JHEP **0108**, 055 (2001) [arXiv:hep-ph/0107316].
- [39] Z. Ahmed *et al.* [CDMS Collaboration], Phys. Rev. Lett. **102**, 011301 (2009); Z. Ahmed *et al.* [The CDMS-II Collaboration], Science **327**, 1619-1621 (2010).
- [40] E. Aprile *et al.* [XENON100 Collaboration], Phys. Rev. Lett. **105**, 131302 (2010). [arXiv:1005.0380 [astro-ph.CO]].
- [41] G. Belanger, F. Boudjema, A. Pukhov and A. Semenov, Comput. Phys. Commun. **180**, 747 (2009) [arXiv:0803.2360 [hep-ph]].

- [42] E. Aprile, The XENON Dark Matter Search, WONDER Workshop, LNGS, March 22, 2010.
- [43] B. Cabrera, “SuperCDMS Development Project”, April 2005.
- [44] H. Baer, C. H. Chen, M. Drees, F. Paige and X. Tata, Phys. Rev. D 591999055014 H. Baer, C. Balázs, A. Belyaev, T. Krupovnickas and X. Tata, JHEP 03062003054; S. Abdullin and F. Charles, Nucl. Phys. **B547**, 60 (1999); S. Abdullin *et al.* [CMS Collaboration], J. Phys. G **28**, 469 (2002) [arXiv:hep-ph/9806366]; B. Allanach, J. Hetherington, A. Parker and B. Webber, JHEP082000017; R. L. Arnowitt, B. Dutta, T. Kamon, N. Koley and D. A. Toback, Phys. Lett. B **639**, 46 (2006) [arXiv:hep-ph/0603128]; D. Feldman, Z. Liu and P. Nath, Phys. Rev. Lett. **99**, 251802 (2007) [arXiv:0707.1873 [hep-ph]]; D. Feldman, Z. Liu, P. Nath and B. D. Nelson, Phys. Rev. D **80**, 075001 (2009) [arXiv:0907.5392 [hep-ph]]; E. Izaguirre, M. Manhart and J. Wacker, arXiv:1003.3886 (2010).
- [45] A. Djouadi, M. M. Muhlleitner and M. Spira, Acta Phys. Polon. B **38**, 635 (2007) [arXiv:hep-ph/0609292].
- [46] K. L. Chan, U. Chattopadhyay and P. Nath, Phys. Rev. D **58** (1998) 096004; R. L. Arnowitt and P. Nath, Phys. Rev. D **46**, 3981 (1992); J. L. Feng, K. T. Matchev and T. Moroi, Phys. Rev. Lett. **84**, 2322 (2000); U. Chattopadhyay, A. Corsetti and P. Nath, Phys. Rev. D **68**, 035005 (2003); H. Baer, C. Balazs, A. Belyaev, T. Krupovnickas and X. Tata, JHEP **0306**, 054 (2003).
- [47] D. Feldman, Z. Liu and P. Nath, Phys. Rev. D **80**, 015007 (2009) [arXiv:0905.1148 [hep-ph]].
- [48] H. Baer, C. h. Chen, F. Paige and X. Tata, Phys. Rev. D **52**, 2746 (1995) [arXiv:hep-ph/9503271].
- [49] I. Hinchliffe, F. E. Paige, M. D. Shapiro, J. Soderqvist and W. Yao, Phys. Rev. D **55**, 5520 (1997) [arXiv:hep-ph/9610544].
- [50] ATLAS Collaboration, Internal Note, ATLAS-COM-CONF-2010-039; CMS Collaboration, Internal Note, CMS PAS JME-09-010; CMS Collaboration, Internal Note, CMS PAS JME-10-004; A. Schwartzman, Performance of Jet, Missing Transverse Energy and Tau Reconstruction with ATLAS in pp Collisions at $\sqrt{s} = 7$ TeV, ICHEP, 2010; J. Weng, Performance of Jet and Missing Transverse Energy Reconstruction with CMS in pp collisions at $\sqrt{s} = 7$ TeV, ICHEP, 2010.